






Cite this: *Chem. Sci.*, 2023, 14, 7988

All publication charges for this article have been paid for by the Royal Society of Chemistry

# Conditional generation of free radicals by selective activation of alkoxyamines: towards more effective and less toxic targeting of brain tumors†

Patricia Piris, <sup>‡a</sup> Duje Buric,<sup>‡a</sup> Toshihide Yamasaki, <sup>b</sup> Paul Huchedé,<sup>c</sup> Maïlys Rossi,<sup>a</sup> Mélanie Matteudi,<sup>a</sup> Marie-Pierre Montero, <sup>a</sup> Anne Rodallec,<sup>a</sup> Romain Appay,<sup>d</sup> Christine Roux,<sup>a</sup> Sébastien Combes,<sup>ae</sup> Eddy Pasquier,<sup>a</sup> Marie Castets,<sup>c</sup> Nicolas André,<sup>af</sup> Paul Brémont <sup>\*ae</sup> and Manon Carré <sup>\*a</sup>

Brain tumors are an important cause of suffering and death. Glioblastoma are the most frequent primary tumors of the central nervous system in adults. They are associated with a very poor prognosis, since only 10% of GBM patients survive 5 years after diagnosis. Medulloblastoma are the most frequent brain malignancies in childhood; they affect the cerebellum in children under 10 years of age in 75% of cases. The current multimodal treatment comes at the expense of serious and often long-lasting side effects. Herein, we propose the synthesis of a library of novel alkoxyamines as anticancer drug candidates. The most efficient molecule, ALK4, was selected based on its ability to inhibit both survival and migration of GBM and MB cells in 2D cultures and in 3D tumor spheroids. A fluorescent derivative was used to show the early cytosolic accumulation of ALK4 in tumor cells. Spontaneous homolysis of ALK4 led to the release of alkyl radicals, which triggered the generation of reactive oxygen species, fragmentation of the mitochondrial network and ultimately apoptosis. To control its homolytic process, the selected alkoxyamine was bioconjugated to a peptide selectively recognized by matrix metalloproteases. This bioconjugate, named ALK4-MMPp, successfully inhibited survival, proliferation, and invasion of GBM and MB tumor micromasses. We further developed innovative brain and cerebellum organotypic models to monitor treatment response over time. It confirmed that ALK4-MMPp significantly impaired tumor progression, while no significant damage was observed on normal brain tissue. Lastly, we showed that ALK4-MMPp was well-tolerated *in vivo* by zebrafish embryos. This study provides a new strategy to control the activation of alkoxyamines, and revealed the bioconjugate ALK4-MMPp bioconjugate as a good anticancer drug candidate.

Received 10th March 2023  
Accepted 28th June 2023

DOI: 10.1039/d3sc01315d

rsc.li/chemical-science

<sup>a</sup>Centre de Recherche en Cancérologie de Marseille (CRCM), Inserm UMR1068, CNRS UMR7258, Aix-Marseille Université U105, Institut Paoli Calmettes – Faculté de Pharmacie, Marseille, France. E-mail: manon.carre@univ-amu.fr

<sup>b</sup>Institut de Chimie Radicale, CNRS UMR7273, Aix-Marseille Université – Faculté des Sciences, Marseille, France

<sup>c</sup>Centre de Recherche en Cancérologie de Lyon (CRCL), Université Claude Bernard Lyon 1, INSERM 1052, CNRS 5286, Centre Léon Bérard, Lyon, France

<sup>d</sup>Service D'anatomie Pathologique et de Neuropathologie, Hôpital de La Timone, Assistance Publique-Hôpitaux de Marseille (APHM), Marseille, France

<sup>e</sup>DOSynth Platform, Centre de Recherche en Cancérologie de Marseille (CRCM), Faculté de Pharmacie, Marseille, France

<sup>f</sup>Service D'hématologie & Oncologie Pédiatrique, Hôpital de La Timone, Assistance Publique-Hôpitaux de Marseille (APHM), Marseille, France

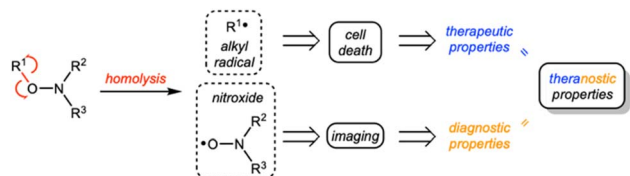
† Electronic supplementary information (ESI) available. CCDC 1413928 and 1413931. For ESI and crystallographic data in CIF or other electronic format see DOI: <https://doi.org/10.1039/d3sc01315d>

‡ Co-first authors.

## Introduction

Alkoxyamines  $R^1-ONR^2R^3$  are small molecules that can undergo homolysis to generate an alkyl radical  $R^1\cdot$  and a nitroxide  $R^2R^3NO\cdot$ . Based on this feature, alkoxyamines have various applications.<sup>1</sup> They have been widely used in polymer chemistry,<sup>2</sup> particularly as initiators and controls of nitroxide-mediated polymerization.<sup>3</sup> More recently, new strategies have been considered for using alkoxyamines in therapeutics. Alkoxyamines may represent novel theranostic agents since (i) the alkyl radical can trigger the cell death process in cancer cells and (ii) the nitroxide can be used to amplify the Overhauser-enhanced magnetic resonance imaging (OMRI) signal<sup>4,5</sup> (Scheme 1).

We previously demonstrated the ability of the alkoxyamine 4-pyridin-(1-SG1)ethyl-N-methyl-1-ium to reduce the survival of melanoma cells, colon carcinoma cells, glioblastoma cells and leukemia cells.<sup>4</sup> We also showed that a series of imidazole-containing alkoxyamines, for which activation of homolysis was



Scheme 1 General concept using alkoxyamines as theranostic agents.

conducted by protonation or methylation, exhibited proliferation inhibition properties in glioblastoma cells.<sup>6</sup> In addition, alkoxyamines are low molecular weight molecules whose charge,  $pK_a$  and  $\log D_{7.4}$  values can be modulated to regulate their passage across biological membranes.<sup>7</sup> This family of molecules may thus represent a new therapeutic option of choice.

This strategy of using alkoxyamines as anticancer agents could hold promise for the management of brain tumors, which are a major cause of suffering and death. Glioblastomas (GBM) are the leading example, accounting for 50% of all malignant tumors of the central nervous system in adults.<sup>8,9</sup> Standard treatment for newly diagnosed GBM involves surgical resection, followed by radiation therapy and chemotherapy.<sup>10</sup> However, despite this aggressive multimodal treatment, the median survival time is only 15 months and almost all GBMs relapse within or near the initial disease site.<sup>11,12</sup> Medulloblastomas (MB), embryonal tumors of the cerebellum, are the most common malignant brain tumors in childhood. With current multimodal therapy, long-term survival is now achieved in 60–75% of patients,<sup>13</sup> but it comes at the cost of serious side effects that considerably alter the quality of life of children in the long-term.<sup>14</sup> Thus, the common challenge of using alkoxyamines in these intracranial tumors is to maximize the inhibition of cancer cell proliferation and invasion while minimizing deleterious side effects.

In the present work, we synthesized a library of alkoxyamines, among which ALK4 was highlighted as the most effective against human GBM and MB cell lines in 2D culture as well as in 3D tumor spheroids. Fluorescent analogues showed that ALK4 rapidly accumulates in tumor cells and triggers apoptotic cell death mediated by endogenous oxidative stress. The activation of the homolysis was controlled by bioconjugating ALK4 to a short peptide selectively recognized by matrix metalloproteinases (MMPs), which are overexpressed in the tumor microenvironment.<sup>15</sup> Real-time follow-up of tumor progression in innovative brain and cerebellum organotypic models confirmed the benefits of the bioconjugate in inhibiting GBM and MB cell survival and invasion without altering the healthy tissue. Finally, the safety of this bioconjugate *in vivo* was shown in a zebrafish model, further strengthening the interest of this molecule in the future treatment of GBM and MB.

## Results and discussion

### Synthesis and characterization of new alkoxyamines

To generate the library of alkoxyamines, copper-catalyzed coupling of SG1 nitroxide (*N*-(2-methylpropyl)-*N*-(1-diethylphosphono-2,2-dimethylpropyl)-*N*-oxyl) and of benzylic bromide derivatives was performed to obtain thirteen alkoxyamines

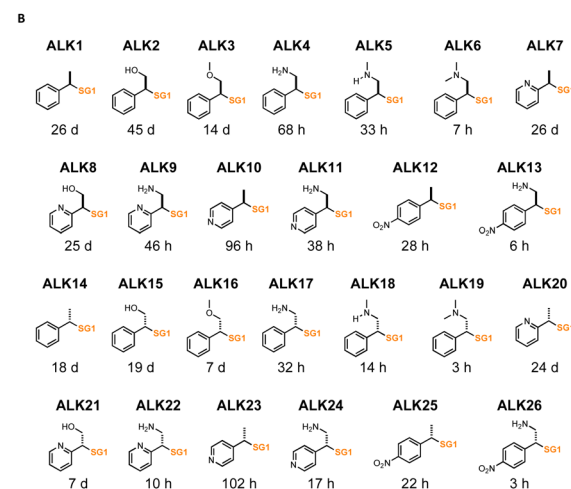
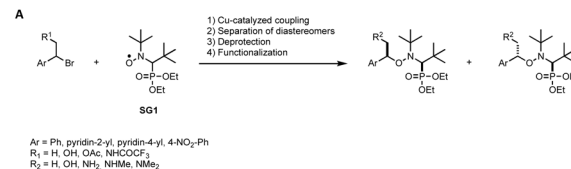


Fig. 1 Library of alkoxyamines. (A) Synthesis of alkoxyamines. (B) Name, structure and estimated half-life time of homolysis at 37 °C of the 26 alkoxyamines investigated in this work.

(Fig. 1A). The diastereoisomers were then separated by column chromatography to obtain pure and diastereoisomerically homogeneous compounds (Fig. 1B). When a protecting group was required, the trifluoroacetamide was preferred, as the deprotection step must be carried out in mild and non-acidic conditions to avoid potential undesired homolysis activated by protonation, which would have considerably altered yields. Therefore, each diastereoisomer were independently hydrolyzed in basic conditions to give deprotected alkoxyamines. We obtained a library of 26 molecules, all based on the same SG1 nitroxide but owning diverse alkyl parts, with aromatic rings (phenyl, 4-nitrophenyl, pyridin-2-yl, pyridin-4-yl) and functionalized methyl groups (Fig. 1B).

These compounds were characterized by NMR (<sup>1</sup>H, <sup>13</sup>C, <sup>31</sup>P) and HRMS to ascertain their chemical structures. They were classified depending on their stereochemistry, ALK14 to ALK26 being the diastereoisomer counterparts of ALK1 to ALK13.

We characterized the kinetics of all alkoxyamines in water using EPR or HPLC. Homolysis rates ( $k_d$ ) were determined, and the corresponding energies of activation ( $E_a$ ) were calculated using Arrhenius equation and the averaged pre-exponential factor  $A = 2.4 \times 10^{14} \text{ s}^{-1}$  to obtain half-life times ( $t_{1/2}$ ) values at 37 °C for each alkoxyamine (Fig. 1B).

### Selection of the most effective alkoxyamines in inhibiting proliferation and migration of brain tumor cells

To evaluate the biological activity of the newly synthesized alkoxyamines, cytotoxicity assays were realized in the human U251-MG and U87-MG cells. ALK7 and ALK20 were excluded



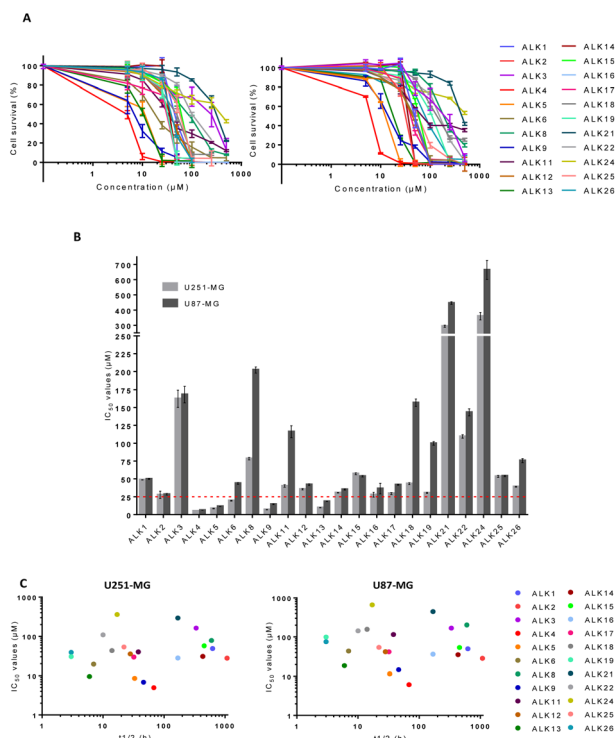


Fig. 2 Cytotoxicity assay of alkoxyamines in U87-MG and U251-MG cells in 2D culture. (A) Survival of U251-MG and U87-MG cells measured by MTT-assay in 2D-cultures, 72 h after treatment with alkoxyamines. (B)  $IC_{50}$  values of alkoxyamines measured by MTT-assay in U87-MG and U251-MG cells. Values are the average of at least three independent experiments  $\pm$  sem. (C) Correlation between  $IC_{50}$  values and half-life time of homolysis at 37 °C of the alkoxyamines.

because of their low aqueous solubility. All other alkoxyamines exerted a dose-dependent inhibition of cell survival in both GBM cell lines after 72 hours of treatment (Fig. 2A). However, the determination of  $IC_{50}$  values – *i.e.*, concentrations that reduce cell survival by 50% – showed significant variations, ranging from  $5.0 \pm 0.1 \mu M$  to  $360 \pm 42 \mu M$  in U251-MG and from  $6.1 \pm 0.1 \mu M$  to  $664 \pm 109 \mu M$  in U87-MG (Fig. 2B). It should be noted that the biological activity of these new alkoxyamines was not correlated to their half-time life, as we previously suggested for other alkoxyamines.<sup>16</sup> For instance, ALK9 whose homolysis process is 4.6 times slower than that of its diastereoisomer ALK22 ( $t_{1/2}$  of 46 h and 10 h, respectively) is 10 times more active in U87-MG cells ( $IC_{50}$  of  $14.5 \pm 0.9 \mu M$  and  $143.2 \pm 8.5 \mu M$ , respectively) (Fig. 2C).

ALK4, ALK5, ALK9 and ALK13 were the most effective, with  $IC_{50}$  values below  $25 \mu M$  in both cell lines (dotted line in Fig. 2B). ALK4 was identified as the most effective in inhibiting U251-MG and U87-MG cell survival, with  $IC_{50}$  of  $5.0 \pm 0.1 \mu M$  and  $6.1 \pm 0.1 \mu M$ , respectively (Fig. 2B). The enantiomers of ALK4 were obtained after separation on preparative chiral HPLC. The two enantiomers of ALK4 were tested towards U87-MG and U251-MG cells. No difference in activity was observed between (*RS*)-ALK4 and (*SR*)-ALK4 –  $IC_{50}$  of 9 and  $7 \mu M$  in U87-MG ( $p > 0.05$ , data not shown) – so the study was continued using the racemic mixture of ALK4.

To determine whether ALK4 was effective in MB cells, we measured its cytotoxic capabilities in ONS-76, HDMB-03 and UW228-2 cell lines. Our data showed that ALK4 was also efficient against the three human MB cell lines, with  $IC_{50}$  of  $16.5 \pm 0.7 \mu M$ ,  $16.3 \pm 2.2 \mu M$  and  $15.2 \pm 1.6 \mu M$ , respectively (Fig. S1A†).

Overall, ALK4, ALK5, ALK9 and ALK13 were significantly more active in tumor cells than any alkoxyamine previously reported in the literature. We previously demonstrated the ability of an alkoxyamine, 4-pyridin-(1-SG1)ethyl-*N*-methyl-1-ium, to reduce the survival of U87-MG cell cultures.<sup>3</sup> However, this first molecule required concentrations 50 times higher than ALK4 in the same cell model. Likewise, a series of imidazole-containing alkoxyamines exhibited less cytotoxic activity against glioblastoma cell lines.<sup>5</sup> More recently, Seren S. *et al.* reported a new series of alkoxyamines, based on phenol or aniline cores, that also inhibited U87-MG cell survival but with  $IC_{50}$  values 25 times higher than ALK4 in the same cell model.<sup>16</sup>

To further investigate ALK4, ALK5, ALK9 and ALK13 anti-cancer properties, a Transwell assay was carried out. It showed that the alkoxyamines were also effective in inhibiting GBM cell

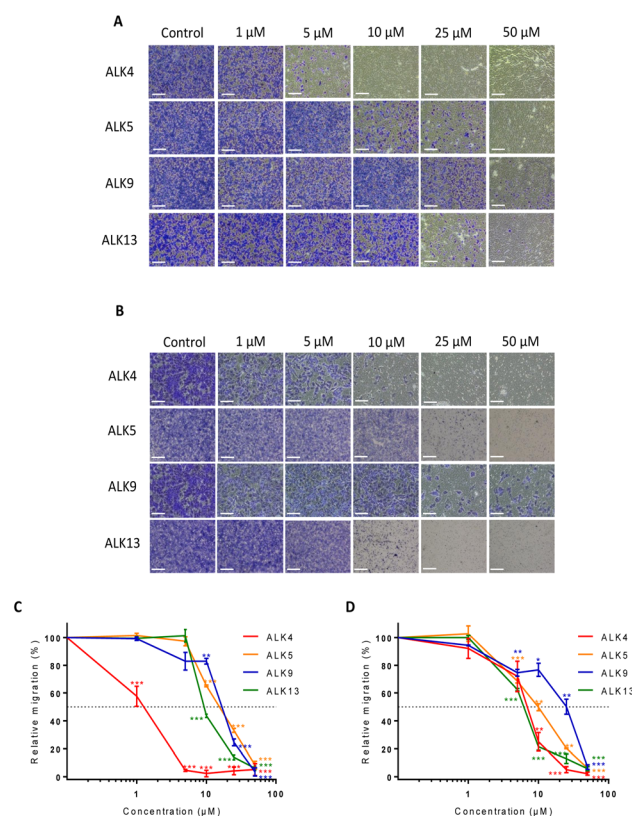


Fig. 3 Impact of ALK4, ALK5, ALK9 and ALK13 on the migration potential of U87-MG and U251-MG cells after 12 hours of treatment. Representative pictures of migrated (A) U87-MG and (B) U251-MG cells without treatment and after 12 hours of treatment with ALK4, ALK5, ALK9 and ALK13. Scale bar = 150  $\mu m$ . Quantification of the anti-migratory effect of ALK4, ALK5, ALK9 and ALK13 in (C) U87-MG and (D) U251-MG cells. Results are expressed as a relative percentage of migrated cells after 12 hours of treatment *versus* migrated cells non-exposed to treatment. Values are the average of at least three independent experiments  $\pm$  sem. \* $p < 0.05$ ; \*\* $p < 0.01$ ; \*\*\* $p < 0.001$ .



migration at low doses (Fig. 3A and B). The results support a superior activity of ALK4, which was able to completely suppress the migratory capacities of U87-MG and U251-MG cells from 5 and 25  $\mu\text{M}$ , respectively (Fig. 3C and D). Thus, the four alkoxyamines revealed by these selection steps show both anti-proliferative and anti-migratory potential in brain tumor cells, making these compounds good candidates for further investigation.

### ALK4 is highly active in GBM and MB tumor spheroids

Multicellular spheroids are 3D structures that are more relevant than cell monolayers to study growth and drug response of tumor masses. We exposed spheroids of DsRed-expressing GBM cells to ALK4, ALK5, ALK9 and ALK13. Fluorescence monitoring showed that each of the molecules reduced GBM spheroid growth over time in a concentration-dependent manner (Fig. 4 and S1†). ALK4 was the most active in both 3D models combined. After four days of treatment, it decreased by  $55 \pm 5\%$  and  $77 \pm 3\%$  the growth of U251-MG spheroids at 5  $\mu\text{M}$  and 10  $\mu\text{M}$ , respectively (Fig. 4A–C). The same ranking of the molecules was obtained when evaluated in U87-MG spheroids, with a decrease of growth by  $56 \pm 3\%$  and

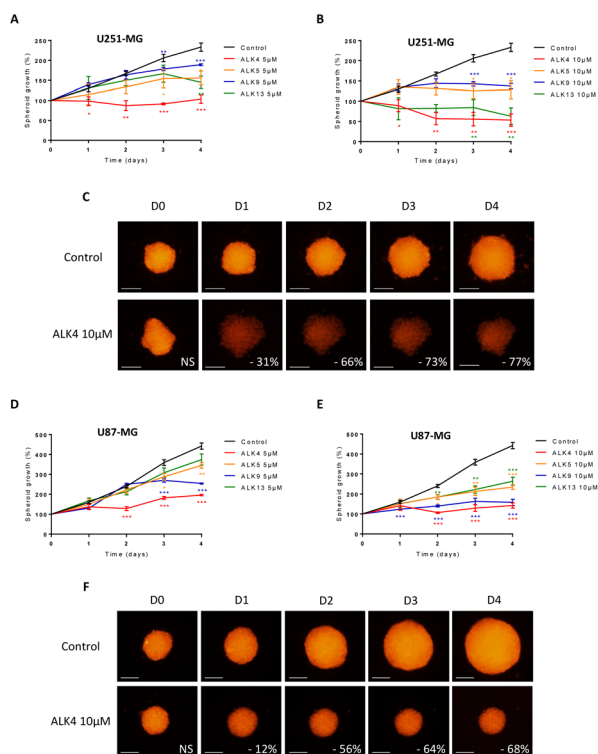


**Fig. 4** Evaluation of the efficacy of ALK4, ALK5, ALK9 and ALK13 at 10  $\mu\text{M}$  in U251-MG and U87-MG GBM spheroids. Monitoring of the growth of U251-MG spheroids (A and B) and U87-MG spheroids (D and E) by fluorescence quantification for 4 days after treatment with ALK4, ALK5, ALK9 and ALK13 at 5  $\mu\text{M}$  and 10  $\mu\text{M}$ . treatment efficacy was expressed as a percentage of spheroid growth inhibition vs. control spheroids. Values are the average of at least three independent experiments  $\bar{x} \pm \text{sem}$ . \* $p < 0.05$ ; \*\* $p < 0.01$ ; \*\*\* $p < 0.001$ . Representative pictures over time of (C) U251-MG and (F) U87-MG spheroids non-treated or exposed to ALK4 at 10  $\mu\text{M}$ . Images were obtained by fluorescence microscopy ( $\lambda_{\text{ex}}$  580 nm/ $\lambda_{\text{em}}$  620 nm). Scale bar = 250  $\mu\text{m}$ .

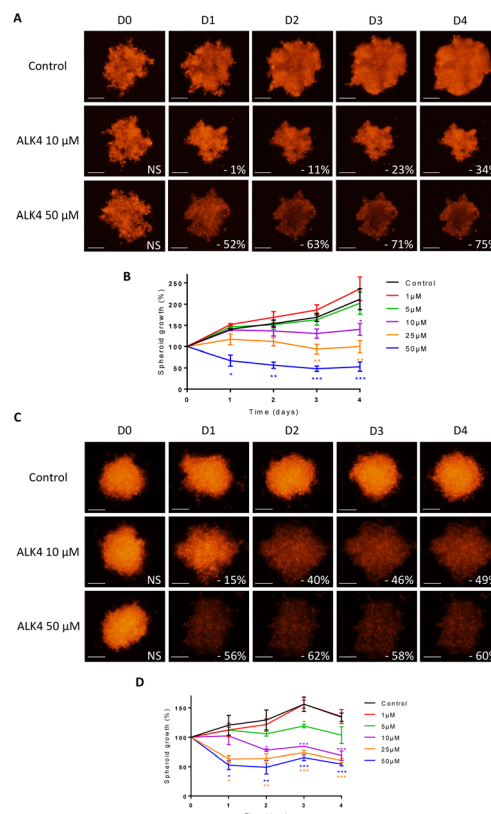


**Fig. 5** Evaluation of the efficacy of ALK4 in MB spheroids. Representative pictures over time of (A) HD-MB03 and (C) ONS-76 spheroids non-treated or exposed to ALK4 at 10  $\mu\text{M}$  and 50  $\mu\text{M}$ . Images were obtained by fluorescence microscopy ( $\lambda_{\text{ex}}$  580 nm/ $\lambda_{\text{em}}$  620 nm). Scale bar = 250  $\mu\text{m}$ . Monitoring of the growth of (B) HD-MB-03 and (D) ONS-76 spheroids by fluorescence quantification for 4 days after treatment with ALK4 at growing concentrations. Treatment efficacy was expressed as a percentage of spheroid growth inhibition vs. control spheroids. Values are the average of at least three independent experiments  $\bar{x} \pm \text{sem}$ . \* $p < 0.05$ ; \*\* $p < 0.01$ ; \*\*\* $p < 0.001$ .

$68 \pm 5\%$  at day 4 for 5  $\mu\text{M}$  and 10  $\mu\text{M}$ , respectively (Fig. 4D–F). The exposure of the two GBM spheroid models to 1, 25 and 50  $\mu\text{M}$  of ALK4 further confirmed that it is the most effective alkoxyamine in GBM tumor micromasses (Fig. S1B–D†).

The efficacy of ALK4 was then tested in MB 3D micromasses. HD-MB03 and ONS-76 spheroid growth were stably suppressed overtime from 10  $\mu\text{M}$  of ALK4 (Fig. 5A–D), validating in these two MB spheroid models that ALK4 is highly active in brain tumor micromasses.

Until now, a few studies had revealed the anticancer potential of alkoxyamines in 2D cell cultures. Here, the use of 3D spheroids that recapitulate tumor architecture and biological characteristics has highlighted the superior anti-tumor activity of ALK4, which will be the focus of subsequent investigations.

### ALK4 can pass through the plasma membrane thanks to its globular shape

While the efficacy of the alkoxyamines in tumor cells is not correlated with their respective half-life time (Fig. 2C), the most active alkoxyamines exhibit the same stereochemistry, rather



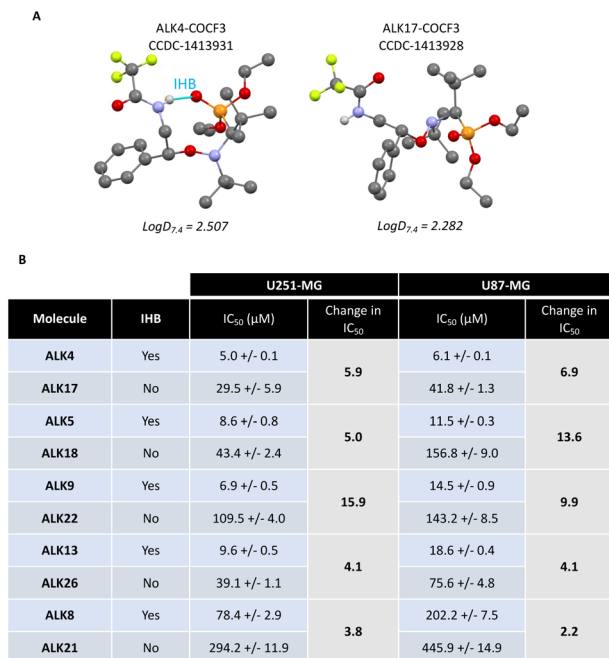


Fig. 6 Comparison of activity between couple of diastereoisomers. (A) Structures of ALK4-COCF<sub>3</sub> and ALK17-COCF<sub>3</sub> obtained after X-ray crystallography, and their logD<sub>7.4</sub> (shake-flask method). (B) Table of IC<sub>50</sub> values of alkoxyamines and ratio in IC<sub>50</sub> values between diastereoisomers. IHB = intramolecular hydrogen bond.

suggesting a stereochemical advantage. Indeed, single-crystal X-ray diffraction of the trifluoroacetamide of ALK4 revealed that it has a globular shape, while the trifluoroacetamide of its diastereomer ALK17 has an open shape (Fig. 6A). The globular conformation is likely to be due to the existence of an intramolecular hydrogen bond (IHB) between the NH and the P=O groups, thus locking the conformation of the alkoxyamine. Moreover, <sup>31</sup>P NMR spectroscopy showed significant differences in chemical shifts between ALK4 and ALK17 (see ESI†). Noteworthy, the IHB can also exist in the other three alkoxyamines of interest – ALK5, ALK9 and ALK13 – versus their corresponding diastereoisomers – ALK18, ALK22, ALK26 – as they all have the required stereochemistry and the required amine function (Fig. 6B). Thus, a globular shape induced by the presence of an IHB may result in alkoxyamines with increased cytotoxic properties, while an open shape may result in a significant loss of activity. This was illustrated, for example, by the 6- and 7-fold higher IC<sub>50</sub> values of ALK17 compared with ALK4 in U251-MG and U87-MG cells, respectively (Fig. 6B). In support of the link between the stereochemistry and activity of the molecules, we previously reported an IHB by X-ray and <sup>31</sup>P NMR in ALK8,<sup>17</sup> the latter being also more cytotoxic than its diastereoisomer ALK21 in GBM cells (Fig. 6B).

To better understand how the globular form of ALK4 can result in an improved activity, we synthesized fluorescent derivatives of ALK4 and ALK17 by coupling the alkoxyamines with FITC (Fig. 7A and B). We first checked that the two FITC-derivatives emitted equal fluorescence signal intensity in cell culture medium (Fig. 7C). By fluorescence microscopy, we then

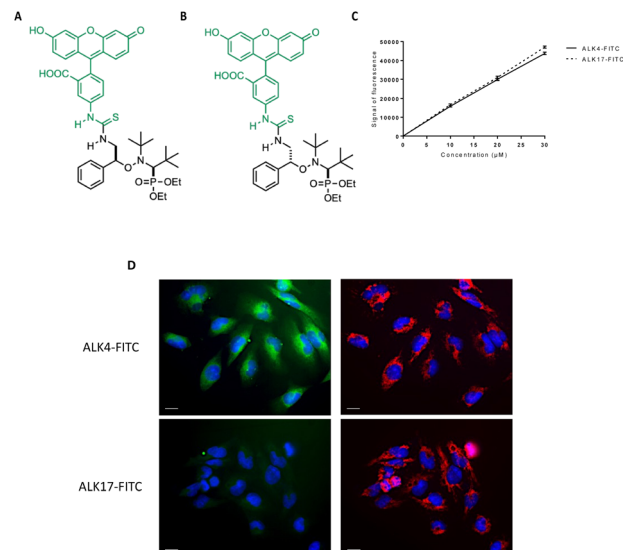


Fig. 7 Study of the intracellular incorporation of ALK4 in GBM cells. Structure of (A) ALK4-FITC and (B) ALK17-FITC. (C) Fluorescence calibration range of ALK4-FITC and ALK17-FITC measured by spectrofluorimetry (PHERAstar, λ<sub>ex</sub> 495 nm/λ<sub>em</sub> 519 nm). (D) Pictures of U251-MG cells observed by fluorescence microscopy (40X objective) after 2 hours of treatment with ALK4-FITC and ALK17-FITC at 15 μM. Left panel: nuclear staining by DAPI (λ<sub>ex</sub> 340 nm/λ<sub>em</sub> 450 nm) and ALK4-FITC analysis within cells (λ<sub>ex</sub> 495 nm/λ<sub>em</sub> 519 nm). Right panel: nuclear staining by DAPI (λ<sub>ex</sub> 340 nm/λ<sub>em</sub> 450 nm) and mitochondrial network analysis by using mtDsRed fluorescence (λ<sub>ex</sub> 580 nm/λ<sub>em</sub> 620 nm). Scale bar = 50 μm.

observed the intracellular accumulation of ALK4-FITC in U251-MG cells expressing mitochondrial DsRed (mtDsRed), already 2 hours after treatment initiation (Fig. 7D). Thanks to DAPI staining of nuclei and mtDsRed labeling of mitochondria, we could observe that ALK4-FITC accumulates within the cytoplasm. In contrast, no fluorescence was observed in the GBM cells exposed to ALK17-FITC. The ability of ALK4 to penetrate cells and exert its activity is therefore linked to its globular form.

While the half-life is not a direct predictive factor of the cytotoxic potential of the alkoxyamines, the structure–activity relationship seems to be based mainly on their 3D structure. Thus, if the substituent linked to SG1 (such as NH<sub>2</sub> or OH) leads to the formation of an IHB, it is very likely that the alkoxyamine will be able to cross biological membranes and therefore be active. This may explain why alkoxyamines in which the formation of the IHB is prevented, by elimination of the heteroatom or introduction of OMe for example, are low-activity molecules.

### Alkyl radicals are responsible for ALK4-mediated oxidative stress and apoptosis of tumor cells

Since alkoxyamine homolysis leads to the release of a nitroxyl radical and an alkyl radical, we evaluated their relative roles in ALK4 activity on brain cancer cells. We first showed that the nitroxide SG1 did not significantly reduce U251-MG and U87-MG cell survival after 72 hours of treatment, even at high concentrations (Fig. 8A and S2A†). The same conclusion was



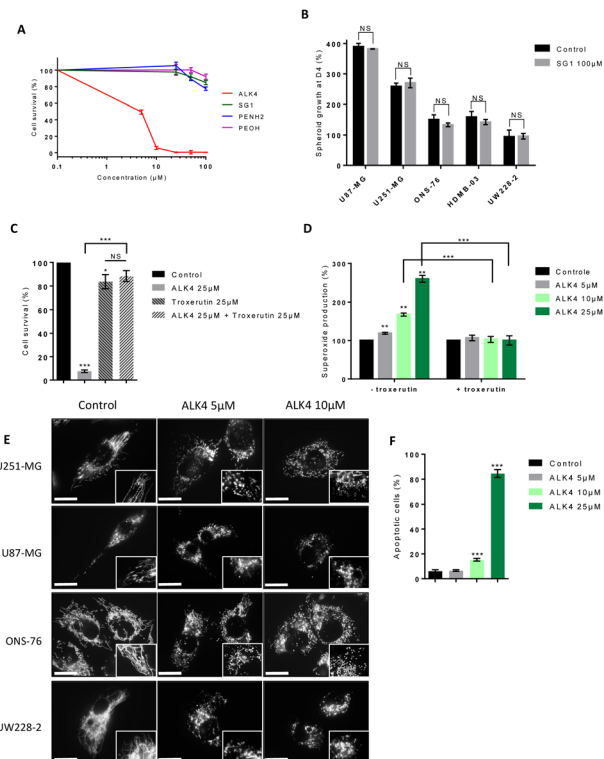


**Fig. 8** Study of the mechanism of action of ALK4. (A) Cell survival measured by MTT-assay after 72 hours of treatment with ALK4, its nitroxide SG1 and its alkyl radical on inactive forms PEA and PEA-OH, in 2D-culture of U251-MG cells. (B) Measurement of glioblastoma and medulloblastoma spheroid growth 4 days after treatment with SG1 at 100  $\mu\text{m}$  compared to control spheroid growth. (C) Survival of U251-MG cells co-exposed to ALK4 and the alkyl scavenger troxerutin (72 hours) in 2D-culture. (D) Superoxide production in 2D-cultures of U251-MG cells upon treatment with ALK4 alone and in combination with troxerutin at 25  $\mu\text{m}$  for 6 hours. (E) Mitochondrial network of U87-MG, U251-MG, ONS-76 and UW228-2 cells observed by fluorescence microscopy (40X objective, mtDsRed fluorescence,  $\lambda_{\text{ex}}$  580 nm/ $\lambda_{\text{em}}$  620 nm) 6 hours after treatment with 5  $\mu\text{m}$  and 10  $\mu\text{m}$  of ALK4. (F) Measurement of apoptosis induction in U251-MG cells after a 48 hours-treatment with ALK4. Scale bar = 50  $\mu\text{m}$ . \* $p < 0.05$ ; \*\* $p < 0.01$ ; \*\*\* $p < 0.001$ .

obtained using two models of GBM spheroids and three models of MB spheroids exposed to SG1 (Fig. 8B), confirming that the alkoxyamine activity was not due to the nitroxide radical.

Then, to determine whether the alkyl radical of ALK4 was responsible of its cytotoxic effect, we used troxerutin, a flavonoid that acts as an alkyl radical scavenger. Troxerutin neutralized the effects of ALK4 (25  $\mu\text{M}$ ), inhibiting its impact on U251-MG and U87-MG cells by more than 80% (Fig. 8C and S2B†). This confirmed that, like most alkoxyamines, ALK4 is active in tumor cells *via* the release of alkyl radicals. In addition, we tested the alkyl part in two non-radical forms: a reduced form phenethylamine (PEA) and an oxidized form DL- $\beta$ -hydroxyphenethylamine (PEA-OH). Both compounds showed low efficacy compared to ALK4, with  $\text{IC}_{50}$  values of 287  $\mu\text{M}$  and 282  $\mu\text{M}$  for PEA and PEA-OH in U251-MG cells, respectively (Fig. 8A). Similar results were obtained in U87-MG cells

(Fig. S2A†). Thus, the efficacy of ALK4 in the brain cancer cells results specifically from the alkyl moiety in its radical form.

Analysis of reactive oxygen species (ROS) levels with the WST1 probe further showed that ALK4 induced a dose-dependent overproduction of endogenous superoxides in cells after 6 hours of treatment (Fig. 8D and S2C†). This effect was counteracted by troxerutin, indicating that alkyl radicals from ALK4 homolysis are responsible for the induction of an oxidative stress in GBM cells.

High levels of ROS in cells can induce oxidative stress and lead to cell death by fragmentation of the mitochondrial network and activation of the intrinsic mitochondrial pathway of apoptosis.<sup>18,19</sup> Accordingly, a fragmentation of the mitochondrial network was shown by fluorescent microscopy in GBM and MB cells after 6 hours of treatment with ALK4 (Fig. 8E).

While the target(s) of the alkyl radicals has not yet been identified, the WST-1 assay used here is specific for the production of superoxide anions by the mitochondrial respiratory chain, which strongly suggests that the alkyl radicals released by the alkoxyamines probably affect oxidative phosphorylation first. The fragmentation of the mitochondrial network a few hours after the start of treatment supports the hypothesis of early targeting of mitochondria and also suggests that the membranes of these organelles are affected by their own production of ROS.

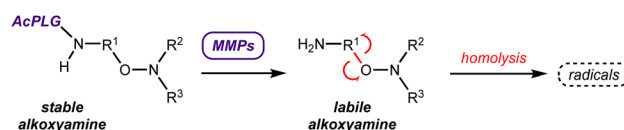
Lastly, cell labelling with annexin V-FITC showed that tumor cell death occurs by induction of the apoptotic program following treatment with ALK4 (Fig. 8F and S2D†).

### Bioconjugation of ALK4 with an MMP-targeted peptide controls its cytotoxic activity

Our strategy was then to control homolysis of the alkoxyamine by conjugation to a peptide specifically recognized by matrix metalloproteinases (MMPs), which are overexpressed by tumor cells *in vivo*.<sup>14</sup> Therefore, bioconjugation of ALK4 was conducted in order to control the release of its radical (Scheme 2).

The tripeptide Ac-Pro-Leu-Gly (Ac-PLG), referred as MMPP, is a well-known sequence recognised and cleaved by MMP enzymes.<sup>20</sup> The bioconjugate ALK4-MMPP was therefore synthesized (Fig. 9A). ALK4 was also bioconjugated to the peptide Suc-Ala-Ala-Pro-Phe (Suc-AAPE, referred as CHYMOp), specifically cleaved by chymotrypsin, an enzyme that is not expressed in GBM and MB microenvironment. The resulting bioconjugate ALK4-CHYMOp was used as a negative control (Fig. 9A).

Our data showed a significant loss of cytotoxicity of ALK4 when conjugated to CHYMOp peptide in two GBM spheroid



**Scheme 2** Use of the MMPs to control the release of the alkoxyamines.

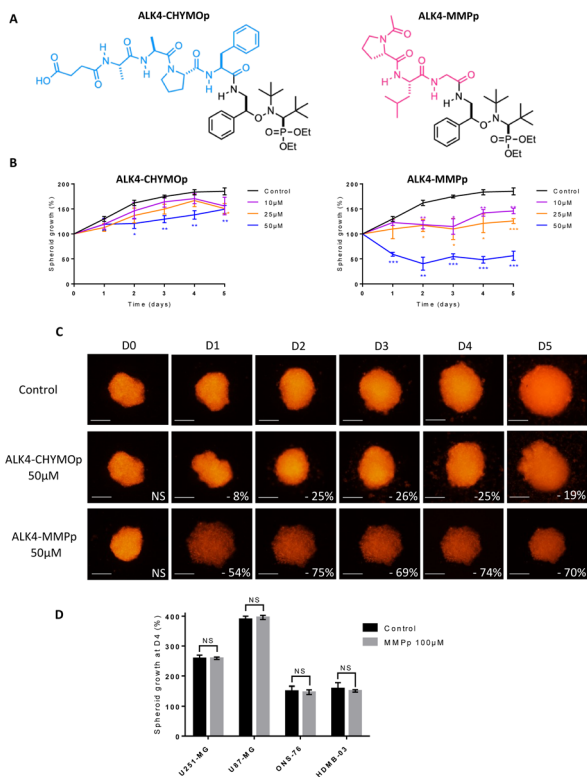


**Fig. 9** Evaluation of the efficacy of the bioconjugates ALK4-CHYMOp and ALK4-MMPp in GBM spheroids. (A) Structure of the bioconjugates ALK4-CHYMOp and ALK4-MMPp. (B) Monitoring of the growth of U251-MG spheroids by fluorescence quantification for 4 days after treatment with ALK4-CHYMOp and with ALK4-MMPp. Treatment efficacy was expressed as a percentage of spheroid growth inhibition vs. control spheroids. Values are the average of at least three independent experiments  $\pm$  sem. \* $p$  < 0.05; \*\* $p$  < 0.01; \*\*\* $p$  < 0.001. (C) Representative pictures over time of U251-MG spheroids non-treated or exposed to 50  $\mu$ M of ALK4-CHYMOp and ALK4-MMPp. Images were obtained by fluorescence microscopy ( $\lambda_{\text{ex}}$  580 nm/ $\lambda_{\text{em}}$  620 nm). Scale bar = 250  $\mu$ m. (D) Measurement of GBM and MB spheroid growth 4 days after treatment with MMPp peptide (100  $\mu$ M) compared to control spheroid growth.

models and two MB spheroid models (Fig. 9B, C and S3A–D $\dagger$ ), confirming that the bioconjugation with the peptide inactivates the alkoxyamine. More importantly, we showed that the treatment with the bioconjugate ALK4-MMPp induced a dose-dependent reduction in U251-MG spheroids growth (Fig. 9B and C). Similar results were obtained in U87-MG, ONS-76 and HD-MB03 spheroid models (Fig. S3A–D $\dagger$ ). The peptide was not cytotoxic when used alone (Fig. 9D), thus confirming that only the alkoxyamine, once released from the bioconjugate, has an activity towards GBM and MB cells after its spontaneous homolysis.

This strategy of coupling alkoxyamines to a peptide to design prodrugs of interest is not limited to the targeting of MMPs and could be adapted to other enzymes overexpressed in the tumor microenvironment. It has been very recently shown that anilide- and phenol-alkoxyamines conjugated to the quadriptide Ala-Ala-Pro-Val also released radicals upon activation by the human-neutrophil elastase.<sup>15</sup> Although the efficacy of these

bioconjugates on 2D cultures of U87-MG cells was found to be 25-fold lower than the one proposed here, this work helps to pave the way for future discoveries on the unexplored potential of alkoxyamines.

### The bioconjugate ALK4-MMPp significantly reduces tumor progression and does not induce damages to healthy brain tissues in organotypic models

To evaluate the potential of ALK4-MMPp in even more biologically-relevant conditions, we developed organotypic cultures in which GBM and MB spheroids stably expressing the fluorescent protein DsRed were grafted onto slices of mouse brain and cerebellum, respectively.

The presence of tumor masses induced a 3.1-fold overproduction of MMPs compared with healthy tissue (Fig. S4A $\dagger$ ). These innovative co-cultures were exposed to ALK4-MMPp two times a week and tumor progression was analyzed over time.

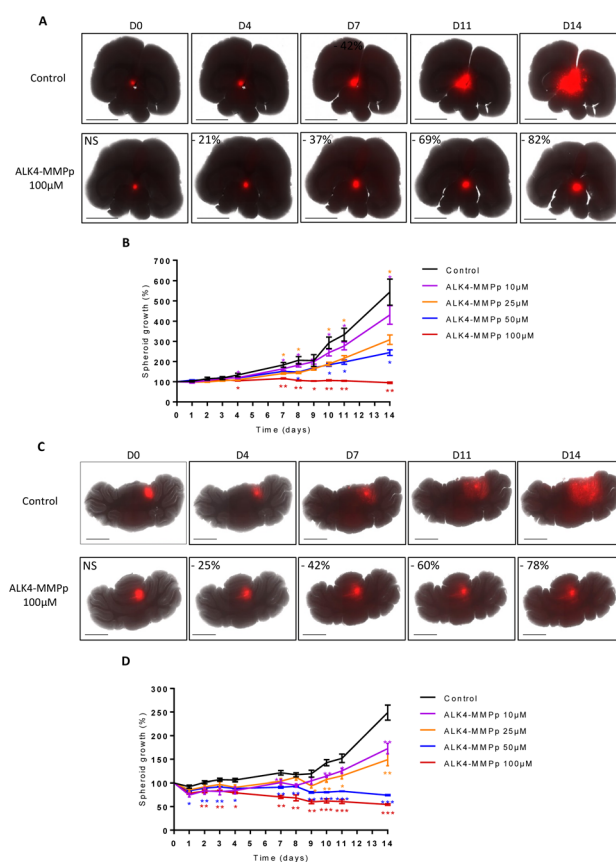


**Fig. 10** Evaluation of the bioconjugate ALK4-MMPp in GBM and MB organotypic models. Representative pictures over 14 days of (A) U251-MG and (C) ONS-76 organotypic models non-treated or exposed to 100  $\mu$ M of ALK4-MMPp (treatment at D0, D4, D7 and D10). Images were obtained using the JuLi<sup>TM</sup>Stage live imaging system ( $\lambda_{\text{ex}}$  580 nm/ $\lambda_{\text{em}}$  620 nm, stitching mode 5  $\times$  6). Scale bar = 2500  $\mu$ m. Monitoring of the growth of (B) U251-MG and (D) ONS-76 spheroids in organotypic brain and cerebellar models by fluorescence quantification for 14 days after treatment with ALK4-MMPp. Values are the average of at least three independent experiments  $\pm$  sem. \* $p$  < 0.05; \*\* $p$  < 0.01; \*\*\* $p$  < 0.001.



Our data showed that the bioconjugate reduced the progression of U251-MG tumor masses in a time and concentration-dependent manner (Fig. 10A and B). For instance, 25  $\mu\text{M}$  of ALK4-MMPP reduced the growth of GBM masses in organotypic models by  $23 \pm 3\%$  and  $43 \pm 3\%$  after 7 days and 14 days respectively ( $p < 0.05$ ). The benefits of ALK4-MMPP were confirmed in organotypic cerebellar models transplanted with ONS-76 tumor masses, with a significant inhibition of MB cell proliferation and invasion over time (Fig. 10C and D). Conversely, the ALK4-CHYMOP bioconjugate did not induce any reduction in tumor mass in this *ex vivo* model (Fig. S4B†), confirming that MMPs are required to regulate ALK4 homolysis and thus control its activation.

After completion of the experiment, organotypic cultures were fixed, sectioned, and subjected to HES staining (Fig. 11A). Microscopic analysis of this staining showed that ALK4-MMPP (even at 100  $\mu\text{M}$ ) did not induce histological damage in non-tumor brain tissue, including the periphery of the GBM mass. Moreover, the  $\gamma\text{H2AX}$  staining of the organotypic models showed that the bioconjugate also did not induce DNA damage in non-tumor brain tissue either (Fig. 11A). Cells within the tumor mass exposed to ALK4-MMPP presented a highest degree of DNA damage, as evidenced by  $\gamma\text{H2AX}$  staining (Fig. 11A-inset), which is consistent with the induction of the oxidative stress by the treatment.<sup>21</sup> This indicates that the treatment is effective in significantly reducing tumor masses without inducing additional damage to the brain.

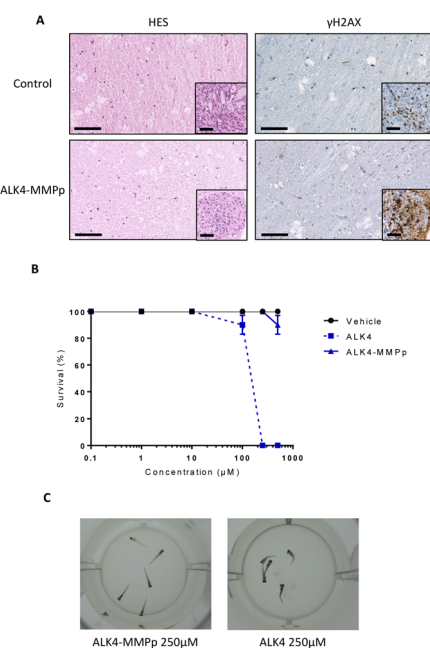


Fig. 11 Analysis of the toxicity of ALK4 and ALK4-MMPP. (A) HES staining and  $\gamma\text{H2AX}$  immunostaining of U251-MG organotypic model after 14 days of treatment with the bioconjugate ALK4-MMPP. Scale bar = 100  $\mu\text{m}$ . (B) Study of toxicity of ALK4 and ALK4-MMPP in zebrafish, 5 fishes per well. Values are the average of at least three independent experiments  $\pm$  sem. (C) Representative pictures of live (left) and dead (right) zebrafishes.

## ALK4-MMPP is well-tolerated by zebrafish embryos *in vivo*

Zebrafish embryos can be employed as a powerful tool to assess toxicity of new pharmaceutical compounds *in vivo*.<sup>22</sup> After being exposed to ALK4 or ALK4-MMPP, from 0.1 to 500  $\mu\text{M}$  for 72 h, surviving zebrafish embryos were counted. Our data show that ALK4 did not significantly impact their survival up to 100  $\mu\text{M}$ , but that the molecule is uniformly lethal at higher concentrations (Fig. 11B and C). In contrast, ALK4-MMPP is not lethal to zebrafish embryos over the entire dose range tested ( $p > 0.05$ ; Fig. 11B). Overall, our results indicate that the ALK4-MMPP bioconjugate is a well-tolerated new compound with anti-tumor activity.

## Conclusions

Alkoxyamines have been widely used in polymer chemistry<sup>2</sup> but have only revealed their cytotoxic potential in the last decade. These molecules remained to be optimized, both to improve their efficacy in tumor cells, but also to control their activation in order to limit their side effects. In this study, we designed and characterized a panel of new alkoxyamines, and selected ALK4 as the molecule with the highest activity against GBM and MB cells and spheroids. Due to its globular shape, ALK4 can accumulate in tumor cells and efficiently trigger apoptosis in a ROS-dependent manner. By conjugating the alkoxyamine to a tripeptide selectively recognized by MMP enzymes, we were able to control its activity. The ALK4-MMPP bioconjugate inhibits the progression of GBM and MB tumor masses over time, without inducing damage to non-tumor tissue. Moreover, it is well tolerated by zebrafish embryos, even at high concentrations. Overall, we have highlighted a new alkoxyamine which, as a bioconjugate, has attractive anti-cancer properties. Our approach at the chemistry–biology interface thus paves the way for the development of future alkoxyamines with potential clinical applications.

## Experimental section

### Synthesis

All details regarding the synthesis of alkoxyamines are described in the ESI.†

### Cell culture

The U87-MG and U251-MG human glioblastoma cancer cell lines were obtained from ATCC (Manassas, VA, USA). They were cultured in Dulbecco's modified eagle's medium (DMEM) supplemented with 10% of Fetal Bovine Serum (FBS) and 100  $\mu\text{g mL}^{-1}$  of penicillin–streptomycin (PS). The human MB cell lines HD-MB03 were kindly provided by Sonia Martial and Gilles Pagès from the Institute for Research on Cancer and Aging (Nice, France). The human ONS-76 and UW228-2 cell lines were kindly provided by Janet Lindsey and Steven Clifford from the Wolfson Childhood Cancer Research Center (New Castle, UK). ONS-76 cells were cultured in Roswell Park Memorial Institute medium (RPMI), supplemented with 10% of FBS and 100  $\mu\text{g mL}^{-1}$  of PS. HD-MB03 cells were maintained in RPMI medium supplemented with 10% of FBS, 100



$\mu\text{g mL}^{-1}$  of PS and with 1% of non-essential amino acids. UW228-2 cells were maintained in DMEM/F12 medium supplemented with 10% of FBS and  $100 \mu\text{g mL}^{-1}$ . All the cells were maintained at  $37^\circ\text{C}$  and 5%  $\text{CO}_2$ .

A mtDsRed plasmid has been transfected in each cell line using Lipofectamine 2000 (Invitrogen, ref. 11668019) following the manufacturer's protocol. Stable transfectants were obtained after Geneticin selection ( $0.8 \text{ mg mL}^{-1}$ , Gibco, ref. 10131035) and two cycles of fluorescence-activated cell sorting (FACS).

All the cells were tested for the absence of mycoplasma contamination (MycoAlert<sup>TM</sup>, Lonza) at least once a month.

### Cytotoxicity test

Stock solutions of each alkoxyamine were prepared in DMSO at 0.15 M and stored at  $-20^\circ\text{C}$ .

Cells were seeded in 96-well plates with 3000 cells per well for U87-MG and U251-MG cells, 2000 cells per well for ONS-76 and UW228-2 cells, 9000 cells per well for HD-MB03. After 24 hours, cells were treated with a range of concentrations of alkoxyamines (500, 250, 100, 50, 25, 10, 5 and  $1 \mu\text{M}$ ) in their respective growth medium for 72 h. The highest concentration of DMSO of which cells were exposed to was 0.002%.

After a 72 h-treatment, cell survival was measured by incubating the GBM and MB cells for 1 h in the medium replenished with  $0.5 \text{ mg mL}^{-1}$  of MTT (3-(4,5-dimethylthiazol-2-yl)-2,5-diphenyl tetrazolium bromide). Medium was replaced by DMSO and optical density (OD) was measured by a microplate spectrophotometer at 550 nm. For each dose of each alkoxyamine tested, results were expressed as percentage of survival cells, according to the following equation:  $\text{OD}_{\text{treated cells}} \times 100 / \text{OD}_{\text{control cells}}$ . The  $\text{IC}_{50}$  values, *i.e.*, concentrations that inhibit 50% of cell survival, were determined using the GraphPad Prism software. All experiments were performed at least in triplicate.

The cytotoxicity test in the presence of the free radical scavenger was carried out with a ALK4 concentration of  $25 \mu\text{M}$  and an incubation time of 1 h. U87-MG and U251-MG cell viability was measured *versus* equal concentration of the nontoxic radical scavenger trihydroxyethylrutin (troxerutin, Santa Cruz Biotechnology, Inc.).

### Spheroid growth assay

DsRed-expressing GBM and MB cells were plated in round bottom 96-well microplates (1000 cells per well for U87-MG – 1200 cells per well for HD-MB03 – 1500 cells per well for UW228-2 and U251-MG – 2000 cells per well for ONS-76) in a culture medium containing 20% methyl cellulose (Sigma-Aldrich, ref. M7027) for 72 h. Spheroids were then exposed to the alkoxyamines. Spheroid growth over time was quantified by acquisition of DsRed fluorescence signal for 4 consecutive days using the PHERAstar<sup>®</sup> FS multi-plate reader ( $\lambda_{\text{ex}}$  580 nm/ $\lambda_{\text{em}}$  620 nm – “well scanning” mode  $10 \times 10$ ). Images were captured with the 4X objective of the JuLI<sup>TM</sup> Stage live imaging system (NanoEntek).

### Transwell<sup>®</sup> migration assay

Migration potential of U87-MG and U251-MG cells was assessed using Transwell<sup>®</sup> migration assay during treatment with the

selected alkoxyamines. In the upper chamber of the Transwell<sup>®</sup> system,  $5 \times 10^4$  cells per chamber were plated on a filter (pore size of  $8 \mu\text{m}$ ) in  $200 \mu\text{L}$  of medium without serum. Cells migrated for 12 hours towards the lower chamber of the Transwell<sup>®</sup> system containing medium with 10% FBS and the alkoxyamines. Non-migrating cells were removed from the upper side of the filter using a cotton swab. Filters were then fixed in 1% glutaraldehyde for 10 minutes, stained with Crystal Violet and imaged with a light microscope. To quantify the migration potential of the cells, filters were immersed in DMSO and concentration of Crystal Violet was determined by spectrometry at 550 nm. Data are expressed as the relative percentage of cells migrating in the presence of the alkoxyamines *versus* control, according to the following equation:  $\text{OD}_{\text{treated cells}} \times 100 / \text{OD}_{\text{control cells}}$ .

### Fluorescence microscopy of FITC derivatives

U251-MG GBM cells were seeded on LabTek II 8-well plates (4000 cells per well) for 48 hours and exposed to a range of concentration of the fluorescent derivatives ALK4-FITC and ALK17-FITC. Two hours after the initiation of the treatment, cell nuclei were stained with DAPI and a fixation of the cells was made, allowing their observation by fluorescence microscopy (40X objective, Leica Biosystems).

### Observation of the mitochondrial network

Stably fluorescent GBM and MB cells were seeded on LabTek II 8-well plates (6000 cells per well for U87-MG and U251-MG cells, 4000 cells per well for ONS-76 and UW228-2 cells) for 48 h and exposed to a range of concentrations of ALK4. 2 hours after the initiation of the treatment, cells were observed by fluorescence microscopy (40X objective, Leica Biosystems).

### Measurement of superoxide production

U251-MG and U87-MG GBM cells were seeded on 96-well microplates (3000 cells per well) for 24 h and exposed to ALK4 or to combination of ALK4 and Troxerutin alkyl scavenger for 6 h. Superoxide anion production was assessed by adding 10% v/v of WST-1 reagent (Roche, ref. 11644807001) in the wells for 30 min at  $37^\circ\text{C}$ . Absorbance was measured at 450 nm with a PHERAstarFS multi-plate reader. To normalize superoxide production to the cell number in each condition, cells were fixed with 1% glutaraldehyde and stained with a solution of 1% (W/V) crystal-violet in 20% methanol (Sigma-Aldrich). The dye has finally been solubilized in DMSO to measure absorbance at 600 nm.

### Annexin V-FITC/PI staining assay

Following a 48 h-treatment, cells were exposed to ApoScreen Annexin V-FITC apoptosis kit (Clinisciences) used according to the manufacturer's instructions. The fluorescence was analyzed by flow cytometry analysis on The Gallios Flow Cytometer (Beckman Coulter) and data were analyzed by Kaluza software (Beckman Coulter).



## Brain and cerebellar organotypic models

To establish organotypic cultures of, we use immunocompetent Swiss mice over 12 weeks old. Brains and cerebellums were surgically harvested and sectioned into 250  $\mu\text{m}$  thick slices using a vibrating blade microtome (Vibratome 2000s, Leica Biosystems). A spheroid formed from DsRed-expressing GBM (for brain) or MB (for cerebellum) cells was then grafted onto each cerebellum slice. These organotypic co-culture models were then placed on inserts with 0.4  $\mu\text{m}$  pore size membranes (Falcon®, ref. 353090) and maintained in a medium containing 50% MEMa, 25% horse serum (Gibco, ref. 16050122), 25% Hanks' Balanced Salt Solution (HBSS; Gibco, ref. 14065056), 10 mM HEPES buffer (Gibco, ref. 15630106), 28 mM Glucose (Gibco, ref. 15023021), 1% L-Glutamine (Gibco, ref. 25030081) and 1% PS. Slices were exposed to a range of concentration of ALK4-MMP or ALK4-CHYMOP every 4 days. Tumor growth and invasion within the cerebellum slices were analysed over time, using the JuLI™ Stage imaging system ( $\lambda_{\text{ex}}$  580 nm/ $\lambda_{\text{em}}$  620 nm – image acquisition with a 4X objective and automated stitching  $5 \times 6$  images) and the PHERAstar® FS multi-plate reader ( $\lambda_{\text{ex}}$  580 nm/ $\lambda_{\text{em}}$  620 nm – fluorescence signal acquisition with a  $15 \times 15$  matrix scanning mode).

## Sample preparation and immunohistochemistry

Samples were fixed overnight at 4 °C with 4% formaldehyde and prepared for paraffin inclusion using automated tissue processor ASP 300 (RRID:SCR\_018916). Dehydration, clarification, and infiltration steps were performed by successive absolute ethanol, histoclear and paraffin baths. After FFPE-embedding, samples were cut at 3  $\mu\text{m}$ -thickness with HM340E microtome (Thermo Scientific). Hematoxylin Eosin Safran staining was performed using automated H&E staining Dako CoverStainer. Ki-67- and  $\gamma\text{H2AX}$ -immunohistochemistry was carried out with rabbit anti-Ki67 antibody (RRID:AB\_443209) and with mouse anti- $\gamma\text{H2AX}$  antibody (Merck Millipore, ref. JBW301) on a Ventana Discovery XT (RRID:SCR\_018643). After deparaffinization, antigen retrieval was performed with Citrate-based buffer pH 6.5 (RiboCC Solution, CC2, ref. 760-107). The primary antibodies were incubated for 20 min at 37 °C then an OmniMap anti-Rabbit HRP Detection Kit (ref. 760-149) was used with DAB. Finally, the counterstaining was done with hematoxylin and slides were cleaned, dehydrated and mounted with permanent mounting media. The microscopic analysis of the tissues was carried out by the pathologists of the Neuropathology Department (Timone Hospital, AP-HM, France).

## MMP dosage assay

The MMP assay was performed using the Amplitude™ Universal Fluorimetric MMP Activity Assay Kit (AAT Bioquest), following the manufacturer's recommendations. 25  $\mu\text{L}$  of the supernatants from the spheroid were collected after 7 days of growth and incubated with 25  $\mu\text{L}$  MMP Green™ substrate working solution for 40 min. The fluorescence signal was then measured with the PHERAstar® FS multi-plate reader ( $\lambda_{\text{ex}}$  490 nm/ $\lambda_{\text{em}}$  525 nm). Values of active MMPs were normalized to the number of surviving MB cells within the spheroid, using the ratio MMP Green/DsRed.

The same procedure was performed with the supernatants of organotypic co-cultures at experiment completion (day 14). Values of active MMPs were normalized to the number of surviving MB cells within the organotypic cultures, using the ratio MMP Green/DsRed.

## Zebrafish

For the *in vivo* toxicity study, AB/TU zebrafish (*Danio rerio*) were raised in a dedicated platform (Zebrafish Rockefeller, Université de Lyon). 48 h post-fertilization (hpf) zebrafish embryos were exposed to a range of concentrations of DMSO, ALK4 or ALK4-MMP directly diluted in culture water (isotonic E3 medium composed of 5 mM NaCl, 0.17 mM KCl, 0.33 mM  $\text{CaCl}_2$ , 0.33 mM  $\text{MgSO}_4$ , methylene blue). Survival was determined by examining and counting alive zebrafish under the microscope (Evos, 10X objective) after 72 h of compound exposition.

## Statistical analysis

All experiments were performed at least in three independent replicates and statistical significance was determined by ANOVA or Student's *t*-test using the GraphPad Prism 6 software. A significant difference between two conditions is defined as:  $*p < 0.05$ ,  $**p < 0.005$ ,  $***p < 0.001$ .

## Data availability

All relevant data are available from the corresponding authors upon reasonable request.

## Author contributions

P. Brémond and M. Carré conceived the idea and supervised the project. P. Piris and D. Buric carried out the chemistry, biology, and pharmacology experiments and analyzed the data. T. Yamasaki assisted in synthesizing and characterizing the alkoxyamines. M-P. Montero and M. Rossi assisted in cell culture and in evaluation of the molecules. A. Rodallec and M. Matteudi helped with the organotypic models. C. Roux conducted the enzymatic dosage. P. Huchedé performed the *in vivo* experiments in zebrafish. R. Appay analyzed the immunohistochemistry experiments. N. André, E. Pasquier, S. Combes and M. Castets assisted in establishing the experimental approach and finalizing the manuscript. M. Carré, P. Piris, P. Brémond, and D. Buric wrote the article. All authors have read, improved and given approval to the final version of the manuscript. P. Brémond, M. Carré and N. André were responsible for funding acquisition.

## Conflicts of interest

There are no conflicts to declare.

## Acknowledgements

We would like to thank S. Vigier for his help with animal experimentation, the Spectropole for NMR and HRMS analyses, N. Vanthuyne for chiral HPLC experiments, M. Giorgi



for X-ray diffraction analyses and the ICEP platform of CRCM for their help in immunohistochemistry experiments. This work was supported by research funding from charities (GEFLUC, RESOP, La Marie-Do, AROU, Association de Recherche contre le Cancer, Ligue Contre le Cancer) and institutions (Canceropôle PACA, Institut National du Cancer and Région Sud). This project has also received funding from the Excellence Initiative of Aix-Marseille University – A\*MIDEX, a French “Investissements d’Avenir” program.

## References

- 1 G. Audran, P. Brémond and S. R. A. Marque, *Chem. Commun.*, 2014, **50**(59), 7921–7928.
- 2 G. Audran, E. Bagryanskaya, S. Marque and P. Postnikov, *Polymers*, 2020, **12**(7), 1481.
- 3 A. Studer and T. Schulte, *Chem. Rec.*, 2005, **5**(1), 27–35.
- 4 D. Moncelet, P. Voisin, N. Koonjoo, V. Bouchaud, P. Massot, E. Parzy, G. Audran, J. M. Franconi, E. Thiaudière, S. Marque, P. Brémond and P. Mellet, *Mol. Pharm.*, 2014, **11**(7), 2412–2419.
- 5 G. Audran, P. Brémond, J. M. Franconi, S. R. A. Marque, P. Massot and P. Mellet, *Org. Biomol. Chem.*, 2014, **12**(5), 719–723.
- 6 T. Yamasaki, D. Buric, C. Chacon, G. Audran, D. Braguer, S. Marque, M. Carré and P. Brémond, *Bioorg. Med. Chem.*, 2019, **27**(10), 1942–1951.
- 7 M. Patel and B. Patel, *CNS Drugs*, 2017, **31**(2), 109–133.
- 8 T. Ostrom, H. Gittleman, G. Truitt, A. Boscia, C. Kruchko and J. Barnholtz-Sloan, *Neuro Oncol.*, 2018, **20**(suppl\_4), iv1–iv86.
- 9 J. Thakkar, T. Dolecek, C. Horbinski, T. Ostrom, D. Lightner and J. Barnholtz-Sloan, *Cancer Epidemiol. Biomarkers Prev.*, 2014, **23**(10), 1985–1996.
- 10 M. Khabibov, A. Garifullin, Y. Boumber, K. Khaddour, M. Fernandez and F. Khamitov, *Int. J. Oncol.*, 2022, **60**(6), 69.
- 11 T. Tykocki and M. Eltayeb, *J. Clin. Neurosci.*, 2018, **54**, 7–13.
- 12 R. Lukas, D. Wainwright, E. Ladomersky, S. Sachdev, A. Sonabend and R. Stupp, *Oncology*, 2019, **33**(3), 91–100.
- 13 A. Thomas and G. Noël, *J. Multidiscip. Healthc.*, 2019, **12**, 335–347.
- 14 V. Bernier and O. Klein, *Neurochirurgie*, 2021, **67**(1), 83–86.
- 15 K. Kessenbrock, V. Plaks and Z. Werb, *Cell*, 2010, **141**(1), 52–67.
- 16 S. Seren, J. P. Joly, P. Voisin, V. Bouchaud, G. Audran, S. Marque and P. Mellet, *J. Med. Chem.*, 2022, **65**(13), 9253–9266.
- 17 G. Audran, R. Bikanga, P. Brémond, M. Edeleva, J. P. Joly, S. R. A. Marque, P. Nkolo and V. Roubaud, *Org. Biomol. Chem.*, 2017, **15**(39), 8425–8439.
- 18 Y. Yang, S. Karakhanova, W. Hartwig, J. D’Haese, P. Philippov, J. Werner and A. Vazhin, *J. Cell. Physiol.*, 2016, **231**(12), 2570–2581.
- 19 U. Sai Srinivas, B. Tan, B. Vellayappan and A. Jeyasekharan, *Redox Biol.*, 2019, **25**, 101084.
- 20 T. Kline, M. Torgov, B. A. Mendelsohn, C. Cervený and P. Senter, *Mol. Pharmacol.*, 2004, **1**(1), 9–22.
- 21 U. Sai Srinivas, B. Tan, B. Vellayappan and A. Jeyasekharan, *Redox Biol.*, 2019, **25**, 101084.
- 22 H. Brown, K. Schiavone, S. Tazzyman, D. Heymann and T. Ja Chico, *Expert Opin. Drug Discov.*, 2017, **12**(4), 379–389.

